Check for updates

Influence of the substitution pattern on exciton localisation in centrosymmetric quadrupolar dyes

Chinju Govind, [ID][a] Kamil Skonieczny, [ID][b] Daniel T. Gryko [ID]*[b] and Eric Vauthey [ID]*[a]

Localisation of the electronic excitation *via* excited-state symmetry breaking (ESSB) is a characteristic property of many quadrupolar dyes in polar environments, and was shown to depend on the nature of the electron donor (D) and acceptor (A) subunits and their separation distance. Here, we compare the excited-state properties of two centrosymmetric D−π−A−π−D dyes with a dipyrrolonaphthyridinedione (DPND) acceptor and *N,N*-dimethylaniline donors, which only differ by the position of the −π−D arms on the DPND core. Time-resolved IR spectroscopy reveals that ESSB and hence exciton trapping on single A−π−D branch is facilitated with the donor arms in 1 and 7 positions on the DPND core compared to 3 and 9 positions, given that it occurs in a medium polar solvent for the former and only in highly polar media for the latter. This *a priori* unexpected difference is explained by the significantly larger dipole moment generated upon ESSB for the 1,7 isomer, as reflected by its much larger fluorescence solvatochromism compared to the other isomer. In this respect, the DPND core with its C_{2h} symmetry allows for a much finer tuning of the excited-state properties of quadrupolar dyes than most previously used D or A cores of higher symmetry.

1 Introduction

Over the past few years, excited-state symmetry breaking (ESSB) in polar environments was found to be a common phenomenon of many multipolar molecules consisting of electron donor (D)–acceptor (A) branches arranged in D–$(\pi$–A$)_{2,3}$ or A–$(\pi$–D$)_{2,3}$ motifs.[1–32] During this process, the exciton, initially distributed evenly over the whole molecule, localises, at least partially, on one D–π–A branch. As a consequence, the excited state changes from quadrupolar/octupolar to dipolar. Previous investigations revealed that the propensity of a multipolar molecule to undergo ESSB in polar solvents increases with the electron donating and withdrawing strength of the D and A constituents as well as with their separation distance. These results were rationalised with a simple excitonic model in which ESSB is only possible if the loss of interbranch coupling, V_{ib}, upon localisation is compensated by a gain in solvation energy.[27,33–35] The effect of substitution pattern was also investigated by comparing two D−π−A−π−D molecules with the same D and A subunits but with different symmetries, one centrosymmetric and linear and the other with the two branches forming a right angle.[36] Full localisation of the excitation on

one branch was found to be easier, *i.e.* to require a less polar solvent, for the linear molecule than for the right-angled one. This was explained by the fact that the delocalised state of the right-angled molecule is already polar. Consequently the gain in solvation energy upon ESSB is smaller than for the linear one.

Here, we compare two formally centrosymmetric D−π−A−π−D molecules, which differ by the position of the π–D branches on the dipyrrolonaphthyridinedione (DPND) acceptor core, *i.e.*, in either 1 and 7 positions, '**A**way' from the pyrrole N atom (**A1**) or in 3 and 9 positions, '**C**lose' to the pyrrole N atom (**C1**, Fig. 1). DPNDs are recently introduced cross-conjugated dyes,[37] and are now well recognised for their strong and tunable emission,[38,39] large two-photon absorption cross-section,[40]
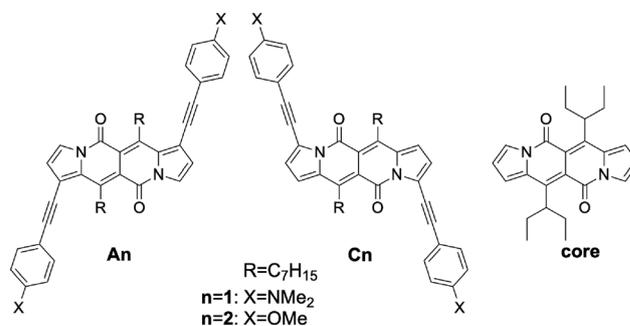
[a] Department of Physical Chemistry, University of Geneva, 30 Quai Ernest-Ansermet, CH-1211 Geneva 4, Switzerland. E-mail: eric.vauthey@unige.ch

[b] Institute of Organic Chemistry, Polish Academy of Sciences, Kasprzaka 44/52, 01-224 Warsaw, Poland. E-mail: daniel.gryko@icho.edu.pl

Fig. 1 Structure of the D−π−A−π−D dyes (**An**, **Cn**) and of the DPND core model.

This journal is © the Owner Societies 2026

Phys. Chem. Chem. Phys., 2026, **28**, 8387–8395 | **8387**

and significant singlet fission yield.[41] As a comparison, molecules **A2** and **C2** with the dimethylanilines replaced by the much weaker donor anisoles as well as the DPND **core** alone were also investigated. To detect occurrence of ESSB, we apply time-resolved IR absorption spectroscopy (TRIR) in the $-C\equiv C-$ stretching region. If electronic excitation is delocalised evenly over the whole molecule, only the anti-symmetric $-C\equiv C-$ vibration is visible in the IR spectrum.[42] On the other hand, as soon as the centro-symmetry of the excited state is lost, the symmetric $-C\equiv C-$ mode becomes IR active as well and two bands are now visible in the transient IR spectrum. We find that ESSB does not occur with anisole units as donors (**A2** and **C2**) but is operative with both **A1** and **C1**. However, our results reveal that the tendency to undergo ESSB depends on the substitution pattern, with **A1** exhibiting a higher propensity than **C1**. This difference is explained by the combination of two effects: (i) a weaker conjugation, hence a smaller interbranch coupling, and (ii) a more dipolar excited state upon ESSB for **A1** compared to **C1**.

2 Experimental

2.1 Dyes

The dyes **C1** and **C2** were synthesised as described in ref. 43, while **A2** was prepared as discussed in ref. 39. The synthesis of **A1** was performed *via* Sonogashira reaction as described in the SI (Fig. S1–S3). The synthesis of **core** will be published separately in due course. The solvents, cyclohexane (CHX, Thermo Scientific), toluene (TOL, Thermo- Scientific), tetrahydrofuran (THF, Thermo Scientific), benzonitrile (BCN, Thermo Scientific), acetonitrile (ACN, Sigma-Aldrich), and dimethyl sulfoxide (DMSO, Roth) were of the highest commercially available purity and were used as received.

2.2 Stationary spectroscopy

Electronic absorption spectra were measured using a Cary 50 spectrometer, whereas emission spectra were recorded on a Horiba FluoroMax-4 spectrofluorometer. The fluorescence spectra were corrected using a set of secondary emissive standards.[44]

2.3 Time-resolved spectroscopy

2.3.1 Time-resolved fluorescence. Fluorescence lifetime measurements were performed using the time-correlated single-photon counting (TCSPC) technique with a home-built setup described in ref. 45. Excitation was achieved with a tunable picosecond laser source (NKT photonics SuperK COMPACT with SuperK SELECT tunable multiline filter). The full width at half maximum (FWHM) of the instrument response function (IRF) was around 200 ps.

2.3.2 Electronic transient absorption spectroscopy. Ultrafast electronic transient absorption (TA) measurements were performed with a setup described in ref. 46 and based on an amplified Ti:Sapphire system (Solstice Ace, Spectra-Physics), producing 35 fs pulses centred at 800 nm with a 5 kHz repetition rate. The pump pulses were generated using a TOPAS-Prime combined with a NirUVis module (Light Conversion). The pump

irradiance on the sample was between 0.15 and 0.75 mJ cm^{-2}. Probing was achieved from about 320 to 750 nm using white light pulses generated in a 3 mm CaF$_2$ plate. The polarisation of the pump pulses was at magic angle with respect to that of the probe pulses. The sample cell was 1 mm thick and the IRF had a FWHM varying between 80 and 350 fs, depending on the probe wavelength.

2.3.3 Time-resolved infra-red spectroscopy. The time-resolved infrared (TRIR) spectroscopy measurements were performed using a setup described in detail previously,[47] and based on an amplified Ti:Sapphire system (Spectra-Physics, Solstice, 100 fs, 800 nm, 1 kHz). The pump pulses were generated from the second harmonic of the output of an optical parametric amplifier (Light Conversion, TOPAS-C). Probing was achieved using the output of an optical parametric amplifier (TOPAS C, Light Conversion) combined with a non-collinear difference-frequency-mixing module (NDFG, Light Conversion). These pulses were dispersed in a Triax 190 spectrograph (Horiba, 150 lines per mm) and detected with a 2×64 elements MCT array (Infrared Systems Development). The samples were flowed through a cell with CaF$_2$ windows separated by a 500 μm spacer and had an absorbance of less than 0.3 at the excitation wavelength.

2.4 Quantum-chemical calculations

All calculations were carried out in the gas phase at the density functional theory (DFT) or time-dependent (TD) DFT level using the CAM-B3LYP functional,[48] combined with the 6-31G(d,p) basis set, as implemented in the Gaussian 16 (rev.B) package.[49]

3 Results

3.1 Stationary spectroscopy and quantum-chemical calculations

The electronic absorption and emission spectra of **A1** and **C1** in different solvents are depicted in Fig. 2. The lowest energy absorption band of both dyes in CHX exhibits a distinct vibronic structure that becomes hardly visible in polar solvents due to broadening. This band shifts to lower energy by 1100 cm^{-1} when going from **A1** to **C1**. Additionally to the broadening, this band exhibits a small solvatochromism, which correlates with the solvent polarisability (Fig. S4), pointing to a non-polar ground state, as expected, and to dispersion as the dominant solute–solvent interactions.[50,51] The lower absorption band of **A2** and **C2** with the weak anisoleD show similar behaviour, except for a weaker broadening in polar solvents (Fig. S5).

Much larger solvatochromism and band broadening can be observed in the fluorescence spectrum of **A1** and **C1** (Fig. 2), whereas only weak solvent dependence is found with **A2** and **C2** (Fig. S5). The red shift of the fluorescence of **A1** and **C1** correlates with the orientational polarisation of the solvent (Fig. S4). This points to a solvatochromism dominated by dipole–dipole interactions,[50] and suggests a dipolar excited state in polar solvents, hence a localisation of the excitation.

8388 | *Phys. Chem. Chem. Phys.*, 2026, **28**, 8387–8395
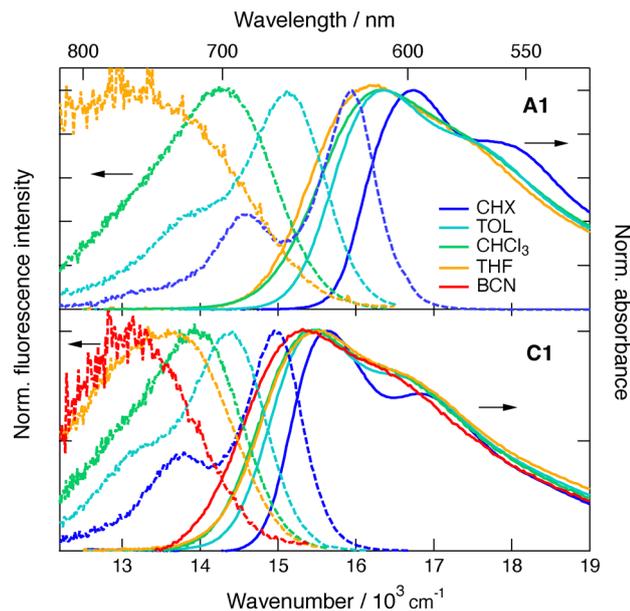
This journal is © the Owner Societies 2026

Fig. 2 Electronic absorption (solid lines) and fluorescence spectra (dashed lines) of **A1** (top) and **C1** (bottom) in various solvents. CHX: cylohexane; TOL: toluene; THF: tetrahydrofuran; BCN: benzonitrile.
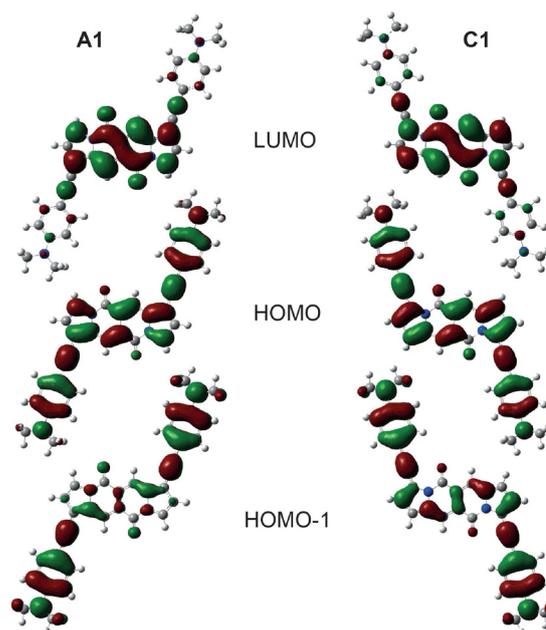

Fig. 3 Frontier molecular orbitals (CAM-B3LYP/6-31G(d,p)) of analogues of **A1** and **C1** with R=H (Fig. 1) involved in the $S_1 \leftarrow S_0$ (HOMO to LUMO) and $S_2 \leftarrow S_0$ (HOMO−1 to LUMO) transitions.

Interestingly, although these two dyes consist of the same D and A subunits at the same distance, the fluorescence solvatochromism of **A1** is significantly larger than that of **C1**, with a shift of 6570 *vs.* 3880 cm^{-1} when going from CHX to BCN (Fig. S4). The solvent shift is also accompanied by a marked decrease in fluorescence quantum yield, which correlates with the shortening of the fluorescence lifetime observed by going from CHX to THF. This effect is more marked with **A1**, namely by a factor of about 5 (2.6 and 0.5 ns) *vs.* a factor of less than 2 (2.8 and 1.5 ns) for **C1**, as shown in Table S1. The fluorescence solvatochromism of **A2** and **C2** is comparatively much smaller, 1400 and 1160 cm^{-1} respectively, when going from CHX to BCN (Fig. S5). Additionally, the fluorescence lifetime is essentially the same in CHX and BCN (Table S1). These results are consistent with the much weaker electron-donating properties of anisole.

The above results can be rationalised using gas-phase quantum-chemical calculations at the (TD)-DFT level of analogues of **A$_n$** and **C$_n$** with the heptyl substituents replaced by H atoms. They point to a planar ground state for **A$_n$** and **C$_n$**. However, significant torsional disorder is predicted, given that these molecules are relative flexible for the rotation around the single bonds of the phenylethynyl arms. For **A1**, the barrier for torsion is slightly lower than for **C1**, namely, 2.0 *vs.* 3.1 k_BT at room temperature (Fig. S7).

According to TD-DFT calculations, the $S_1 \leftarrow S_0$ transition of all four dyes is dominated by a HOMO to LUMO one-electron excitation and characterised by a large oscillator strength, around 1.5–1.6 for **A1** and **C1** and around 1.3 for the other two (Fig. 3 and S8, Table S2). The red shift of the $S_1 \leftarrow S_0$ transition observed when going from **A1** to **C1** (Fig. 2) is also reproduced by the calculations, with the S_1 state of **C1** located 0.11 eV (900 cm^{-1}) below that of **A1** (Table S2). Additionally, the

$S_2 \leftarrow S_0$ transition, mostly a HOMO−1 to LUMO excitation, is predicted to be about 0.6–0.7 eV higher and to be symmetry forbidden. This result is fully consistent with the theoretical models used to describe the lowest excited states of quadrupolar molecules, with the one-photon allowed and two-photon forbidden $S_1 \leftarrow S_0$ transition and the one-photon forbidden and two-photon allowed $S_2 \leftarrow S_0$ transition.[3,27,33,52] In the excitonic model,[53] these dyes can be considered as two D–π–A chromophores arranged in a collinear manner, similar to a J-dimer. The frontier molecular orbitals reveal that these first two electronic transitions involve significant charge transfer from the dimethylanilines D to the DPND core, and point to a significant increase in quadrupole moment upon excitation (Fig. 3). This change is comparatively smaller with anisole as donor, *i.e.* for **A2** and **C2**, as expected (Fig. S8).

TD-DFT calculations also predicted a planar S_1 state, but higher barriers for torsion of the phenylethynyl arms, namely 7 and 8k_BT, for **A1** and **C1**, respectively (Fig. S7). This difference in barrier for torsion between ground and excited states is typical of phenylethynyl-based chromophores and results in non-mirror image relationship of absorption and emission spectra, with a narrower and more structured fluorescence spectrum, as observed here in CHX.[54–57]

3.2 Electronic transient absorption spectroscopy

Electronic transient absorption (TA) measurements were performed with all four dyes in the non-polar CHX and the polar BCN. The TA data were analysed globally assuming a series of successive exponential steps to obtain evolution-associated difference absorption spectra (EADS) and time constants.[46,58] These EADS and time constants do not necessarily correspond
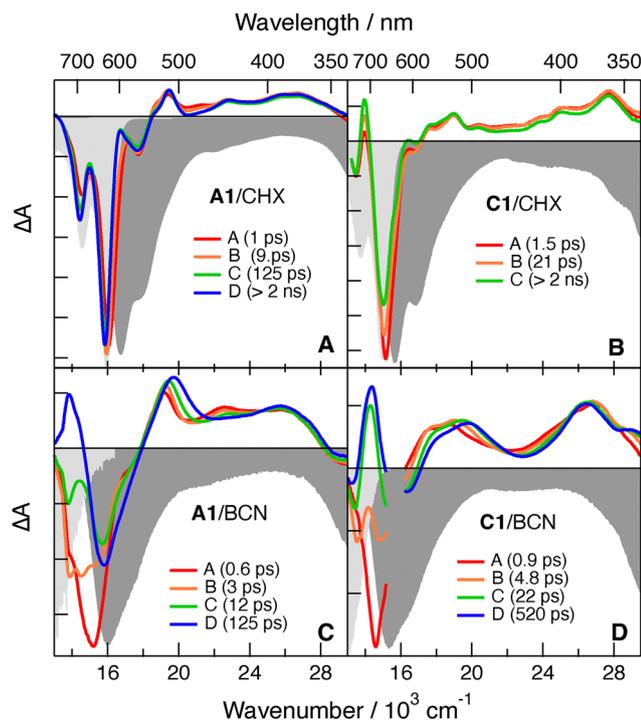
Fig. 4 Evolution-associated difference absorption spectra and time constants obtained from global analysis of the transient absorption data recorded upon photoexcitation of **A1** and **C1** in cyclohexane (CHX, A and B) and benzonitrile (BCN, C and D) assuming a series of successive exponential steps (A → B → ⋯ →). The negative stationary absorption and stimulated emission spectra are shown in shaded area for comparison.

Fig. 5 Evolution-associated difference absorption spectra and time constants obtained from global analysis of the transient absorption data recorded upon photoexcitation of the **core** (A) without and (B) with 1 M *N,N*-dimethylaniline (DMA) in benzonitrile assuming a series of successive exponential steps (A → B → ⋯ →). The negative stationary absorption and stimulated emission spectra are shown in shaded area for comparison.

to well-defined states/species and inverse rate constants but reflect the changes in the TA spectra and their timescales.

The TA spectra recorded with **A1** and **C1** in CHX are qualitatively similar with a negative band above 600 nm due mostly to stimulated emission (SE) and positive bands at shorter wavelength due to $S_{n>1} \leftarrow S_1$ excited-state absorption (ESA) (Fig. 4A, B and S9). The bleach of the $S_1 \leftarrow S_0$ band is hardly visible because of overlapping ESA features. The latter are also overlapping with the lower energy side of the SE of **C1**. Apart from the decay of all bands on the ns timescale, in agreement with the fluorescence lifetimes (Table S1), the TA spectra exhibit only little dynamics at early time, which most probably arise from vibrational and/or structural relaxation. For example, the increasing vibronic structure of the SE band of **A1** is consistent with planarisation.[56]

By contrast, significant spectral dynamics can be observed in BCN, especially in the SE region (Fig. 4C, D and S9). They can be explained by the red shift of the SE band due to solvent relaxation and the appearance of ESA features that are hidden by the SE band at early time. The timescales of these changes are similar to those of solvent relaxation in BCN.[59] The concurrent blue shift of the ESA band around 500 nm is also consistent with the equilibration of the S_1 state and an increase of $S_{n>1}$–S_1 gap. Comparatively, much less spectral dynamics can be observed with **A2** and **C2** (Fig. S10 and S11), in agreement with their markedly smaller fluorescence solvatochromism.
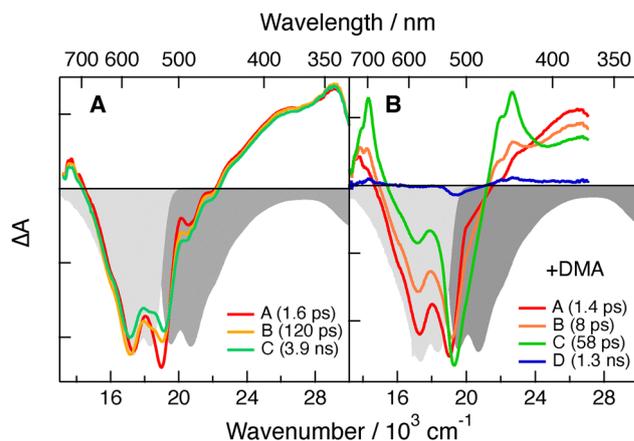
These TA data in BCN also reveal a strong acceleration of the excited-state decay relative to CHX, with the S_1 lifetime decreasing from ns to 125 and 500 ps for **A1** and **C1**, respectively. This decrease with increasing solvent polarity is also consistent with that observed for the fluorescence lifetime when going from CHX to THF. This effect is notably more marked for **A1** than **C1**. Comparatively, the excited-state decays of **A2** and **C2** are not affected by the solvent polarity.

To find spectral evidence for a charge-transfer character of the S_1 state of **A1** and **C1**, TA measurements were also carried with the DPND **core** alone and with 1 M *N,N*-dimethylaniline (DMA) in BCN. As illustrated in Fig. 5, in the presence of DMA, the SE band of **core** decays in a few ps and positive bands around 440 and 700 nm appear concurrently. Given that the radical cation of DMA absorbs relatively weakly around 460–470 nm,[60] these two bands are most probably due to the radical anion of **core**. Based on these results, the ESA features observed with **A1** and **C1** in BCN are consistent with a S_1 state characterised by significant charge transfer from the DMA donor(s) to the DPND acceptor.

3.3 Time-resolved infra-red spectroscopy

Time-resolved IR (TRIR) measurements were carried out with **A1** and **C1** in a series of solvents of increasing polarity (Fig. S12 and S13). **A2** and **C2** were only investigated in CHX and DMSO, as very little solvent dependence of the TRIR dynamics was observed (Fig. S14 and S15). Like for the TA experiments, the TRIR data were analysed globally assuming series of successive exponential steps (Fig. 6, S14 and S15).[58,61] In CHX, both **A1** and **C1** exhibit a single band, ESA1, in the –C≡C– region (Fig. 6). For **A1**, this band is significantly narrower and is shifted by +20 cm^{-1} relative to **C1**. For both molecules, this bands rises and narrows during the first ∼20 ps before decaying on the ns timescale, in agreement with the S_1 state lifetime determined from TA and time-resolved fluorescence. This early

8390 | *Phys. Chem. Chem. Phys.*, 2026, **28**, 8387–8395

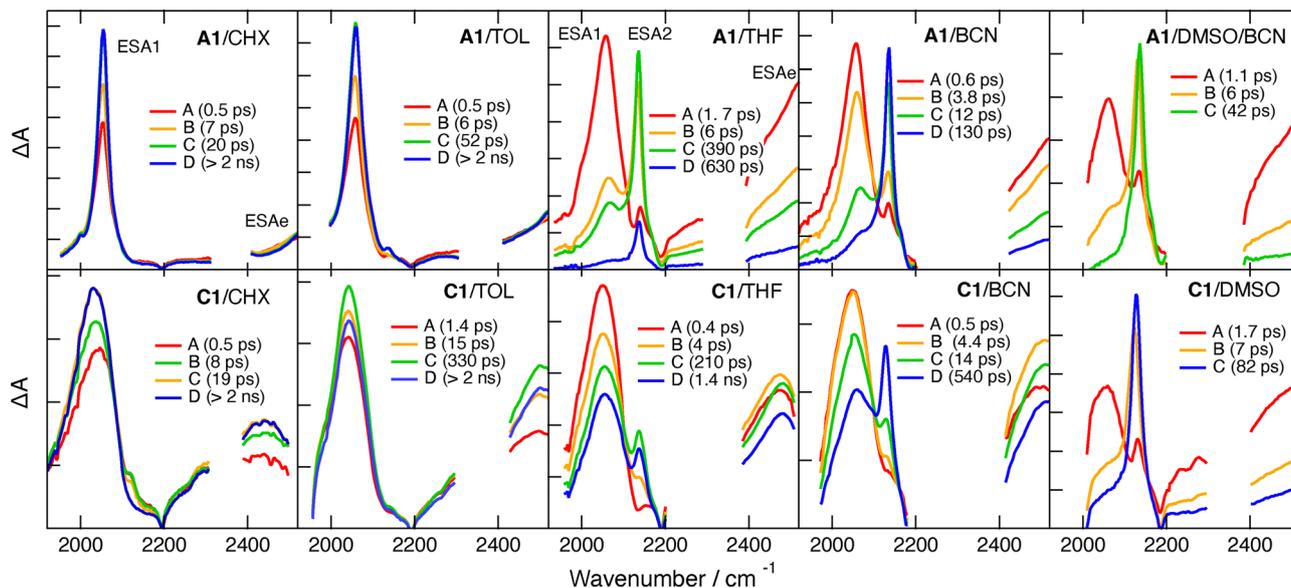This journal is © the Owner Societies 2026

Fig. 6 Evolution-associated difference absorption spectra and time constants obtained from global analysis of the time-resolved IR absorption data recorded upon photoexcitation of **A1** and **C1** in various solvents assuming a series of successive exponential steps (A → B → ··· →). CHX: cyclohexane; THF: tetrahydrofuran; BCN: benzonitrile; DMSO: dimethyl sulfoxide. Given the poor solubility of **A1** in DMSO, a 80 : 20 (v/v) DMSO/BCN mixture was used.

narrowing can be attributed to vibrational and structural relaxation,[62] similarly to the early dynamics observed in the TA spectra. Additionally to ESA1, another broad positive feature is present on the high-frequency side of the weak negative feature around 2200 cm^{-1} due to the ground-state bleach of the $-C\equiv C-$ stretch band (Fig. S6). This high-frequency band, ESAe, which extends above 2600 cm^{-1}, is assigned to a mid-IR electronic transition from the delocalised S_1 state, as supported by the data discussed below.[24,42] ESAe is significantly more intense with **C1** and probably overlaps with ESA1. The mixing of electronic and vibrational transitions with **C1** could possibly be at the origin of the much larger bandwidth of ESA1. As illustrated in Fig. S14 and S15, the TRIR spectra recorded with **A2** and **C2** exhibit similar behaviour.

The presence of a single $-C\equiv C-$ stretching band in the TRIR spectrum points to a symmetric distribution of the excitation on the two D–π–A branches with only the antisymmetric stretching mode IR allowed.[10,42] In principle, the large bandwidth recorded with **C1** could also be due to the presence of two weakly split bands and could, thus, indicate an uneven distribution of the excitation. This can however be excluded by the results obtained in polar solvents, as described below.

The TRIR spectra measured in the weakly polar TOL are very similar to those in CHX (Fig. 6). However, significant changes are observed when increasing solvent polarity to THF as illustrated in Fig. 6. The early spectra recorded with **A1** are dominated by ESA1 at the same frequency as in CHX but with a larger width and by the broad ESAe, which is now as intense as ESA1. Additionally, a weak and relatively narrow vibrational band, ESA2, can be observed on the high-frequency side of ESA1. Over the first 10 ps after excitation, ESA2 increases and becomes dominant, while ESA1 and ESAe decay concurrently. Afterwards, all three bands decay in parallel in 600–700 ps.

The early TRIR spectra measured with **C1** in THF also exhibit intense ESA1 and ESAe and a weak ESA2 (Fig. 6). However, the intensity increase of ESA2 and parallel decrease of ESA1 and ESAe, which occur during the first few ps, is much smaller than for **A1**. Consequently, after these changes, ESA1 and ESAe remain dominant. After these early dynamics, all three bands decay concurrently on the ns timescale.

The presence of two $-C\equiv C-$ stretching bands in THF can be interpreted as evidence of ESSB and a lopsided distribution of the excitation over the molecule.[10,33] Consequently, the symmetric $-C\equiv C-$ stretching mode is no longer IR forbidden. The early dynamics with the increase of ESA2 and partial decrease of the other two bands reflect the ESSB dynamics. They occur on a timescale similar to those of solvent motion in agreement with previous findings that ESSB is driven by a gain in solvation energy.[27,35,63] The difference in the ESA1/ESA2 intensity ratio between **A1** and **C1** suggests that the extent of asymmetry is larger for **A1**. This conclusion is consistent with the stronger intensity decrease of ESAe, attributed to an electronic transition of the delocalised excited state, observed with **A1** compared to **C1**.

Similar early dynamics are observed upon further increasing the solvent polarity, i.e., in BCN and DMSO (Fig. 6). Due to the limited solubility of **A1** in DMSO, measurements with this dye were carried out in a 80 : 20 (v/v) DMSO/BCN mixture. For **A1**, only ESA2 is present in the late spectra, pointing to a full localisation of the excitation on one A–π–D side of the molecule. In this case again, the timescale of the early dynamics are similar to those of solvent motion.[59] By contrast, for **C1** in BCN, both ESA1 and ESAe remain very intense after equilibration, although ESA2 is more visible than in THF. This band becomes dominant only in the highly polar DMSO, but the other two bands are still visible contrary to **A1**.

These results reveal that full ESSB, *i.e.*, exciton trapping on a single branch, is operative with **A1** in BCN and more polar solvents, whereas excitation in **C1** remains partially delocalised.

In agreement with the TA measurements in CHX and BCN, these TRIR data point to a continuous decrease of the relaxed S_1 state lifetime with increasing solvent polarity, namely, from a few ns in CHX to 600, 130 and 42 ps for **A1** in THF, BCN and DMSO/BCN, respectively. This effect is not as marked for **C1**, whose excited-state lifetime changes from a few ns in CHX and THF to 540 and 82 ps in BCN and DMSO.

Comparatively, the TRIR spectra of the molecules with anisole donors, **A2** and **C2**, exhibit little dynamics with a single vibrational band in the –C≡C– stretching region and a possible broad electronic background in CHX as well as in DMSO (Fig. S14 and S15). Moreover, the excited-state lifetime is on the ns timescale in both solvents. These results suggest that electronic excitation remains evenly delocalised independently of the solvent polarity and the position of the π–D arms.
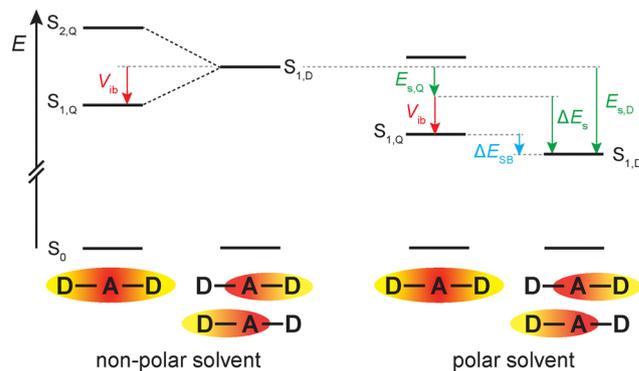

Fig. 7 Energetics of excited-state symmetry breaking. (left) Exciton localisation in non-polar media is not operative because the excitonic stabilisation energy of the delocalised state, V_{ib}, is lost. (right) In polar solvents, the quadrupolar excited state, $S_{1,Q}$, is stabilised by solvation energy, $E_{s,Q}$, which is smaller than $E_{s,D}$, the solvation energy of the dipolar excited state, $S_{1,D}$. If the gain in solvation energy, $\Delta E_s = E_{s,D} - E_{s,Q}$, is larger than V_{ib}, excited-state symmetry breaking is energetically favourable, $\Delta E_{SB} < 0$.

4 Discussion

The trends in the extent of ESSB revealed by the TRIR measurements are fully consistent with the observed fluorescence solvatochromism (Fig. 2 and S5). On the one hand, the negligible solvent dependence of the emission spectra of **A2** and **C2** agrees with a quadrupolar excited state. On the other hand, the substantial emission solvatochromism of **A1** and **C1** points to a dipolar character of the excited state. Furthermore, the larger solvent dependence measured with **A1** compared to **C1** suggests that, in polar media, the excited state of **A1** is more dipolar than that of **C1**.

The absence of ESSB with anisole as donor can be easily explained by its weak electron donating ability, reflected by its very positive oxidation potential of 1.76 V *vs.* SCE relative to 0.78 V *vs.* SCE for DMA.[64,65] These values should be compared with the reduction potential of the DPND of −1.12 V *vs.* SCE,[43] and the energy of its S_1 state of 2.35 eV. According to the Weller equation (eqn (S1)),[66] photoinduced electron transfer between DPND and anisole is highly endergonic, *i.e.* ΔG_{ET} = 0.53 eV, whereas it is energetically favourable with DMA with ΔG_{ET} = −0.45 eV. Therefore, only weak CT from the core to the anisole ends should be expected upon photoexcitation of **A2** and **C2**. Consequently, their S_1 state should be only weakly quadrupolar. By contrast, much larger CT and quadrupolar moment can be expected for the S_1 state of **A1** and **C1**.

More surprising is the finding that ESSB is easier with **A1** than with **C1**, despite them having the same D and A strength and C_{2h} symmetry. To explain this, we consider the simple excitonic model mentioned in the introduction, where both D–π–A–π–D dyes can be approximated to a J dimer of D–π–A with the Davydov splitting of the two lowest delocalised electronic excited states, S_1 and S_2, corresponding to twice the interbranch coupling, $2V_{ib}$ (Fig. 7, left).[27,35] Exciton localisation on a single branch leads to a loss of the interbranch coupling and is, thus, endergonic by V_{ib}. However, if the gain of solvation energy upon

going from the symmetric quadrupolar excited state to the dipolar symmetry-broken state, ΔE_s, exceeds V_{ib}, then ESSB is energetically favourable (Fig. 7, right). As a consequence, the higher tendency of **A1** to undergo ESSB compared to **C1**, must originate from a smaller V_{ib} and/or a larger ΔE_s.

The red shift of the S_1–S_0 absorption and emission spectra of **C1** in CHX relative to those of **A1** (Fig. 2) can be explained by a larger conjugation in the S_1 state of the former and should be associated with a larger V_{ib}. In principle, the splitting of the symmetric and antisymmetric vibrations of two coupled vibrators increases with the magnitude of the coupling.[67,68] Therefore, the larger frequency splitting of ESA2 and ESA1 measured with **C1** relative to **A1** in THF and BCN, namely 85 *vs.* 75 cm^{-1} (Fig. 6), could also reflect a larger V_{ib} value. Finally, calculations of the nucleus-independent chemical shift (NICS) values for **A2** and **C2** reported in ref. 39 predict a slightly higher aromaticity of the pyrrole rings upon 3,9- (*i.e.* **Cn**) than 1,7-substitution (**An**), supporting a higher conjugation for 3,9-substitution and possibly a larger interbranch coupling for **C1**. Nevertheless, all these differences between **An** and **Cn** are small and might not be sufficient to account for the higher tendency of **A1** to undergo ESSB.

However, a major difference between **A1** and **C1** can be observed in the fluorescence solvatochromism, which is more than 50% larger for **A1** (Fig. 2 and S4). This implies that the relaxed S_1 state of **A1** is much more stabilised by polar solvation than that of **C1**, pointing, thus, to a significantly larger gain in solvation energy, ΔE_s, than for **C1**. This higher stabilisation of the relaxed S_1 state of **A1** in polar media is also confirmed by the significantly shorter excited-state lifetime compared to **C1**, *i.e.*, by a faster non-radiative decay due to the reduced S_1–S_0 gap.

The gain in solvation energy, ΔE_s, was shown to be well approximated by taking half of the fluorescence band shift measured by going from a non-polar to a given polar solvent.[27] Based on this, ΔE_s in BCN can be estimated to be larger for **A1**

8392 | *Phys. Chem. Chem. Phys.*, 2026, **28**, 8387–8395

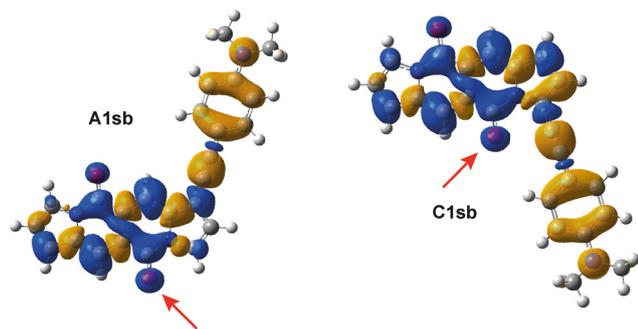This journal is © the Owner Societies 2026

Fig. 8 Charge density difference surfaces calculated for the $S_1 \leftarrow S_0$ transition of single branched analogues of **A1** and **C1**. Yellow and blue colours stand for decrease and increase in electronic density, respectively. The red arrows designate the carbonyl oxygen atom undergoing the largest increase in electronic density upon excitation. For **A1sb**, this atom is located further apart from the electron-donating group, suggesting a more polar excited state than for **C1sb**.

than **C1** by about 0.15 eV. This is a substantial difference that can easily account for the higher propensity of **A1** toward exciton trapping.

The larger ΔE_s of **A1** indicates that the symmetry-broken state of **A1** is more polar than that of **C1**. To try understanding the origin of this effect, we performed quantum-chemical calculations of analogues of **A1** and **C1** but with only a single –π–D branch, namely **A1sb** and **C1sb**. Calculations of the permanent dipole moment of these single-branched molecules predicted unrealistically large values, between 4.5 and 5 D, in the ground state and only a minor increase, around 0.7 D, in the S_1 state. A large ground-state dipole moment is also predicted for **A2sb**, although this molecule exhibits negligible absorption solvatochromism (Fig. S5C), pointing to weak ground state dipole moment. Similar results were obtained with other functionals and basis sets, such as ωB97XD/def2-TZVPP. Reliable calculation of permanent electric dipole moments using standard DFT based methods is known to be problematic for such systems.[69,70] Therefore, the results of these dipole moment calculations were no longer considered.

However, the frontier MOs involved in the $S_1 \leftarrow S_0$ transition as well as the associated charge density difference (CDD) surfaces suggest a possible origin of the higher polarity of the localised S_1 state of **A1**. As illustrated in Fig. 8, the increase of electronic density upon $S_1 \leftarrow S_0$ excitation is not the same for the two carbonyl oxygen atoms. For both **A1sb** and **C1sb**, it is the largest for the carbonyl oxygen located close to the pyrrole ring bearing the –π–D arm. For **A1sb**, this atom is much farther from the DMA donor than for **C1sb**, with a O–N distance of 12.7 Å *vs.* 7.5 Å. Given that dipolar solvation energy scales with the square of the dipole moment, such difference should be sufficient to account for a larger gain in solvation energy upon ESSB in **A1**.

5 Conclusions

Previous investigations of D–(π–A)$_2$ and A–(π–D)$_2$ molecules evidenced how excited-state symmetry breaking and exciton

localisation depend on the push–pull character of the constituents, their separation distance and the overall symmetry of the molecule. The present study with two centrosymmetric D–π–A–π–D dyes, which only differ by the position of the –π–D arms on the DPND acceptor core reveals that the substitution pattern has also an effect on the tendency of the electronic excitation to localise on one A–π–D side in polar media. This difference can be explained by the C_{2h} symmetry of the DPND core. Because of it, substitution of an electron donor in position 3, close to a carbonyl group, or in position 1 away from a carbonyl, leads to different charge-transfer characters in the excited state. Consequently, the dipole moment of the symmetry broken S_1 state is larger when the donors are in positions 1 and 7 (**A1**) than in positions 3 and 9 (**C1**). In this respect, using DPND as a core allows for a finer tuning of the nature of the excited state than most of the donor or acceptors cores used so far, which have a D_{2h} symmetry, and for which substitution on either side is equivalent. These findings illustrate how apparently subtle structural differences can have strong impact on the nature of the excited state of such multipolar dyes. A deeper understanding of these structural effects would certainly facilitate further developments of quadrupolar dyes and fluorophores for specific applications.

Conflicts of interest

There are no conflicts to declare.

Data availability

Supplementary information: synthesis of **A1**, solvatochromism, time resolved fluorescence, transient electronic and IR absorption spectra and global analysis, and quantum-chemical calculations. See DOI: https://doi.org/10.1039/d6cp00121a.

All data can be downloaded from https://doi.org/10.26037/yareta:4qg2qkc5sfdelb65tzyoxzfa6a.

Notes and references

1 S. Amthor, C. Lambert, S. Dümmler, I. Fischer and J. Schelter, *J. Phys. Chem. A*, 2006, **110**, 5204–5214.
2 R. Stahl, C. Lambert, C. Kaiser, R. Wortmann and R. Jakober, *Chem. – Eur. J.*, 2006, **12**, 2358–2370.
3 F. Terenziani, A. Painelli, C. Katan, M. Charlot and M. Blanchard-Desce, *J. Am. Chem. Soc.*, 2006, **128**, 15742–15755.

This journal is © the Owner Societies 2026

Phys. Chem. Chem. Phys., 2026, **28**, 8387–8395 | **8393**

4   F. Terenziani, C. Sissa and A. Painelli, *J. Phys. Chem. B*, 2008, **112**, 5079–5087.

5   S. Easwaramoorthi, J.-Y. Shin, S. Cho, P. Kim, Y. Inokuma, E. Tsurumaki, A. Osuka and D. Kim, *Chem. – Eur. J.*, 2009, **15**, 12005–12017, S12005/1–S12005/11.

6   C. Sissa, A. Painelli, M. Blanchard-Desce and F. Terenziani, *J. Phys. Chem. B*, 2011, **115**, 7009–7020.

7   B. Carlotti, E. Benassi, A. Spalletti, C. G. Fortuna, F. Elisei and V. Barone, *Phys. Chem. Chem. Phys.*, 2014, **16**, 13984–13994.

8   A. Rebane, M. Drobizhev, N. S. Makarov, G. Wicks, P. Wnuk, Y. Stepanenko, J. E. Haley, D. M. Krein, J. L. Fore, A. R. Burke, J. E. Slagle, D. G. McLean and T. M. Cooper, *J. Phys. Chem. A*, 2014, **118**, 3749–3759.

9   B. Carlotti, E. Benassi, C. G. Fortuna, V. Barone, A. Spalletti and F. Elisei, *ChemPhysChem*, 2016, **17**, 136–146.

10 B. Dereka, A. Rosspeintner, Z. Li, R. Liska and E. Vauthey, *J. Am. Chem. Soc.*, 2016, **138**, 4643–4649.

11 B. Dereka, A. Rosspeintner, M. Krzeszewski, D. T. Gryko and E. Vauthey, *Angew. Chem., Int. Ed.*, 2016, **55**, 15624–15628.

12 N. Dozova, L. Ventelon, G. Clermont, M. Blanchard-Desce and P. Plaza, *Chem. Phys. Lett.*, 2016, **664**, 56–62.

13 S. Lee and D. Kim, *J. Phys. Chem. A*, 2016, **120**, 9217–9223.

14 J. S. Beckwith, A. Rosspeintner, G. Licari, M. Lunzer, B. Holzer, J. Fröhlich and E. Vauthey, *J. Phys. Chem. Lett.*, 2017, **8**, 5878–5883.

15 T. M. Cooper, J. E. Haley, D. M. Krein, A. R. Burke, J. E. Slagle, A. Mikhailov and A. Rebane, *J. Phys. Chem. A*, 2017, **121**, 5442–5449.

16 B. Dereka, A. Rosspeintner, R. Stężycki, C. Ruckebusch, D. T. Gryko and E. Vauthey, *J. Phys. Chem. Lett.*, 2017, **8**, 6029–6034.

17 L. G. Łukasiewicz, H. G. Ryu, A. Mikhaylov, C. Azarias, M. Banasiewicz, B. Kozankiewicz, K. H. Ahn, D. Jacquemin, A. Rebane and D. T. Gryko, *Chem. – Asian J.*, 2017, **12**, 1736–1748.

18 Y. Sonoda, *J. Lumin.*, 2017, **187**, 352–359.

19 S. A. Kurhuzenkau, M. Y. Colon Gomez, K. D. Belfield, Y. O. Shaydyuk, D. J. Hagan, E. W. Van Stryland, C. Sissa, M. V. Bondar and A. Painelli, *J. Phys. Chem. C*, 2018, **122**, 5664–5672.

20 B. Bardi, M. Krzeszewski, D. T. Gryko, A. Painelli and F. Terenziani, *Chem. – Eur. J.*, 2019, **25**, 13930–13938.

21 H. Y. Chung, J. Oh, J.-H. Park, I. Cho, W. S. Yoon, J. E. Kwon, D. Kim and S. Y. Park, *J. Phys. Chem. C*, 2020, **124**, 18502–18512.

22 L. G. Łukasiewicz, M. Rammo, C. Stark, M. Krzeszewski, D. Jacquemin, A. Rebane and D. T. Gryko, *ChemPhotoChem*, 2020, **4**, 508–519.

23 X. Niu, Z. Kuang, M. Planells, Y. Guo, N. Robertson and A. Xia, *Phys. Chem. Chem. Phys.*, 2020, **22**, 15743–15750.

24 B. Dereka, D. Svechkarev, A. Rosspeintner, A. Aster, M. Lunzer, R. Liska, A. M. Mohs and E. Vauthey, *Nat. Commun.*, 2020, **11**, 1925.

25 S. L. Bondarev, T. F. Raichenok, S. A. Tikhomirov, N. G. Kozlov, T. V. Mikhailova and A. I. Ivanov, *J. Phys. Chem. B*, 2021, **125**, 8117–8124.

26 A. Cesaretti, A. Spalletti, F. Elisei, P. Foggi, R. Germani, C. G. Fortuna and B. Carlotti, *Phys. Chem. Chem. Phys.*, 2021, **23**, 16739–16753.

27 Z. Szakács, F. Glöcklhofer, F. Plasser and E. Vauthey, *Phys. Chem. Chem. Phys.*, 2021, **23**, 15150–15158.

28 H. Usta, B. Cosut and F. Alkan, *J. Phys. Chem. B*, 2021, **125**, 11717–11731.

29 Z. Wei, S. Sharma, A. M. Philip, S. Sengupta and F. C. Grozema, *Phys. Chem. Chem. Phys.*, 2021, **23**, 8900–8907.

30 M. Fakis, V. Petropoulos, P. Hrobárik, J. Nociarová, P. Osuský, M. Maiuri and G. Cerullo, *J. Phys. Chem. B*, 2022, **126**, 8532–8543.

31 S. Guo, W. Liu, Y. Wu, J. Sun, J. Li, H. Jiang, M. Zhang, S. Wang, Z. Liu, L. Wang, H. Wang, H. Fu and J. Yao, *J. Phys. Chem. Lett.*, 2022, **13**, 7547–7552.

32 B. Dereka, N. Maroli, Y. M. Poronik, D. T. Gryko and A. A. Kananenka, *Chem. Sci.*, 2024, **15**, 15565–15576.

33 A. I. Ivanov, B. Dereka and E. Vauthey, *J. Chem. Phys.*, 2017, **146**, 164306.

34 A. I. Ivanov and V. G. Tkachev, *J. Chem. Phys.*, 2019, **151**, 124309.

35 P. Verma, M. Tasior, P. Roy, S. R. Meech, D. T. Gryko and E. Vauthey, *Phys. Chem. Chem. Phys.*, 2023, **25**, 22689–22699.

36 B. Dereka, E. Balanikas, A. Rosspeintner, Z. Li, R. Liska and E. Vauthey, *J. Phys. Chem. Lett.*, 2024, **15**, 8280–8286.

37 B. Sadowski and D. T. Gryko, *Chem. Sci.*, 2023, **14**, 14020–14038.

38 B. Sadowski, M. F. Rode and D. T. Gryko, *Chem. – Eur. J.*, 2018, **24**, 855–864.

39 K. Skonieczny, L. Kielesinski, M. Grzybowski and D. T. Gryko, *Chem. Commun.*, 2025, **61**, 5602–5606.

40 B. Sadowski, H. Kita, M. Grzybowski, K. Kamada and D. T. Gryko, *J. Org. Chem.*, 2017, **82**, 7254–7264.

41 L. Wang, L. Lin, J. Yang, Y. Wu, H. Wang, J. Zhu, J. Yao and H. Fu, *J. Am. Chem. Soc.*, 2020, **142**, 10235–10239.

42 E. Vauthey, *J. Phys. Chem. Lett.*, 2022, **13**, 2064–2071.

43 M. Grzybowski, I. Deperasińska, M. Chotkowski, M. Banasiewicz, A. Makarewicz, B. Kozankiewicz and D. T. Gryko, *Chem. Commun.*, 2016, **52**, 5108–5111.

44 J. A. Gardecki and M. Maroncelli, *Appl. Spectrosc.*, 1998, **52**, 1179–1189.

45 J. Sissaoui, D. S. Budkina and E. Vauthey, *J. Phys. Chem. Lett.*, 2023, **14**, 5602–5606.

46 J. S. Beckwith, A. Aster and E. Vauthey, *Phys. Chem. Chem. Phys.*, 2022, **24**, 568–577.

47 M. Koch, R. Letrun and E. Vauthey, *J. Am. Chem. Soc.*, 2014, **136**, 4066–4074.

48 T. Yanai, D. P. Tew and N. C. Handy, *Chem. Phys. Lett.*, 2004, **393**, 51–57.

49 M. J. Frisch, G. W. Trucks, H. B. Schlegel, G. E. Scuseria, M. A. Robb, J. R. Cheeseman, G. Scalmani, V. Barone, G. A. Petersson, H. Nakatsuji, X. Li, M. Caricato, A. V. Marenich, J. Bloino, B. G. Janesko, R. Gomperts, B. Mennucci, H. P. Hratchian, J. V. Ortiz, A. F. Izmaylov, J. L. Sonnenberg, D. Williams-Young, F. Ding, F. Lipparini, F. Egidi, J. Goings, B. Peng, A. Petrone, T. Henderson, D. Ranasinghe, V. G. Zakrzewski, J. Gao, N. Rega, G. Zheng, W. Liang, M. Hada, M. Ehara, K. Toyota, R. Fukuda, J. Hasegawa, M. Ishida, T. Nakajima, Y. Honda, O. Kitao,

8394 | *Phys. Chem. Chem. Phys.*, 2026, **28**, 8387–8395

This journal is © the Owner Societies 2026

H. Nakai, T. Vreven, K. Throssell, J. A. Montgomery Jr., J. E. Peralta, F. Ogliaro, M. J. Bearpark, J. J. Heyd, E. N. Brothers, K. N. Kudin, V. N. Staroverov, T. A. Keith, R. Kobayashi, J. Normand, K. Raghavachari, A. P. Rendell, J. C. Burant, S. S. Iyengar, J. Tomasi, M. Cossi, J. M. Millam, M. Klene, C. Adamo, R. Cammi, J. W. Ochterski, R. L. Martin, K. Morokuma, O. Farkas, J. B. Foresman and D. J. Fox, *Gaussian 16 Rev. B.01*, 2016.

50 P. Suppan, *J. Photochem. Photobiol., A*, 1990, **50**, 293–330.

51 T. Renger, B. Grundkötter, M. E.-A. Madjet and F. Müh, *Proc. Natl. Acad. Sci. U. S. A.*, 2008, **105**, 13235–13240.

52 C. Sissa, F. Terenziani and A. Painelli, *J. Phys. Chem. A*, 2008, **112**, 8697–8705.

53 M. Kasha, *Radiat. Res.*, 1963, **20**, 55–70.

54 M. I. Sluch, A. Godt, U. H. F. Bunz and M. A. Berg, *J. Am. Chem. Soc.*, 2001, **123**, 6447–6448.

55 S. J. Greaves, E. L. Flynn, E. L. Futcher, E. Wrede, D. P. Lydon, P. J. Low, S. R. Rutter and A. Beeby, *J. Phys. Chem. A*, 2006, **110**, 2114–2121.

56 I. Fureraj, D. S. Budkina and E. Vauthey, *Phys. Chem. Chem. Phys.*, 2022, **24**, 25979–25989.

57 R. Ringström, F. Edhborg, Z. W. Schroeder, L. Chen, M. J. Ferguson, R. R. Tykwinski and B. Albinsson, *Chem. Sci.*, 2022, **13**, 4944–4954.

58 I. H. M. van Stokkum, D. S. Larsen and R. van Grondelle, *Biochim. Biophys. Acta, Bioenerg.*, 2004, **1657**, 82–104.

59 M. L. Horng, J. A. Gardecki, A. Papazyan and M. Maroncelli, *J. Phys. Chem.*, 1995, **99**, 17311–17337.

60 T. Shida, *Electronic Absorption Spectra of Radical Ions*, Elsevier, Amsterdam, 1988, vol. 34.

61 J. S. Beckwith, C. A. Rumble and E. Vauthey, *Int. Rev. Phys. Chem.*, 2020, **39**, 135–216.

62 P. Hamm, S. M. Ohline and W. Zinth, *J. Chem. Phys.*, 1997, **106**, 519–529.

63 A. E. Nazarov and A. I. Ivanov, *J. Phys. Chem. B*, 2020, **124**, 10787–10801.

64 J. Eriksen and C. S. Foote, *J. Phys. Chem.*, 1978, **82**, 2659–2662.

65 N. Mataga, T. Asahi, Y. Kanda, T. Okada and T. Kakitani, *Chem. Phys.*, 1988, **127**, 249–261.

66 D. Rehm and A. Weller, *Isr. J. Chem.*, 1970, **8**, 259–271.

67 P. Hamm, M. Lim and R. M. Hochstrasser, *J. Phys. Chem. B*, 1998, **102**, 6123–6138.

68 H. Kwon, K. Osawa, J. G. Seol, S. Sung, D. Kim and Y. S. Kim, *J. Chem. Phys.*, 2023, **158**, 214303.

69 A. O. Lykhin, D. G. Truhlar and L. Gagliardi, *J. Chem. Theory Comput.*, 2021, **17**, 7586–7601.

70 H. S. Clifford, M. R. Hennefarth, D. G. Truhlar and L. Gagliardi, *J. Phys. Chem. Lett.*, 2025, **16**, 10400–10409.

This journal is © the Owner Societies 2026

Phys. Chem. Chem. Phys., 2026, **28**, 8387–8395 | 8395